Journal Pre-proof

Experimental and numerical approach of afterburning effects in fuel-rich explosives within confined spaces

Hu Zhou, Ange Lu, Cheng Zheng, Yiwen Wang, Xiangshao Kong, Weiguo Wu

PII: S2214-9147(25)00156-4

DOI: https://doi.org/10.1016/j.dt.2025.05.009

Reference: DT 1665

To appear in: *Defence Technology*

Received Date: 14 January 2025

Revised Date: 18 April 2025

Accepted Date: 12 May 2025

Please cite this article as: Zhou H, Lu A, Zheng C, Wang Y, Kong X, Wu W, Experimental and numerical approach of afterburning effects in fuel-rich explosives within confined spaces, *Defence Technology*, https://doi.org/10.1016/j.dt.2025.05.009.

Experimental and numerical approach of afterburning effects in fuel-rich explosives within confined spaces

Hu Zhou[a,b], Ange Lu[a,b], Cheng Zheng[a,b], Yiwen Wang[a,b],

Xiangshao Kong[a,b,*], Weiguo Wu[a,b]

[a]Green & Smart River-Sea-Going Ship, Cruise and Yacht Research Center, Wuhan University of Technology, Wuhan, 430063, China

[b]School of Naval Architecture, Ocean and Energy Power Engineering, Wuhan University of Technology, Wuhan, 430063, China

[*]***Corresponding author:*** kongxs@whut.edu.cn

Experimental and numerical approach of afterburning effects in fuel-rich explosives within confined spaces

Abstract

The detonation of fuel-rich explosives yields combustible products that persistently burn upon mixing with ambient oxygen, releasing additional energy through a phenomenon known as the afterburning effect. This process greatly influences the evolution of confined blast loading and the subsequent structural response, which is crucial in confined blast scenarios. Given the complex nature of the reaction process, accurate analysis of the afterburning effect remains challenging. Previous studies have either overlooked the mechanisms of detonation product combustion or failed to provide experimental validation. This study introduces a three-dimensional model to effectively characterize the combustion of detonation products. The model integrates chemical reaction source terms into the governing equations to consider the combustion processes. Numerical simulations and experimental tests were conducted to analyze the combustion and energy release from the detonation products of fuel-rich explosives in confined spaces. Approximately 50% of the energy was released during the combustion of detonation products in a confined TNT explosion. Although the combustion of these products was much slower than the detonation process, it aligned with the dynamic response of the structure, which enhanced the explosive yield. Excluding afterburning from the analysis reduced the center-point deformation of the structure by 30%. Following the inclusion of afterburning, the simulated quasi-static pressure increased

by approximately 45%. Subsequent comparisons highlighted the merits of the proposed approach over conventional methods. This approach eliminates the reliance on empirical parameters, such as the amount and rate of energy release during afterburning, thereby laying the foundation for understanding load evolution in more complex environments, such as ships, buildings, and underground tunnels.

Keywords: Blast loading; Numerical simulation; Experimental study; Fuel-rich explosives; Confined space; Afterburning model; Reactive flow

1. Introduction

Fuel-rich explosives inherently contain insufficient oxygen to achieve the complete oxidation of elements during detonation, resulting in the production of combustible intermediates such as CO, CH_4, H_2, and carbon [1]. Common fuel-rich explosives include TNT, RDX, and PETN, which have been extensively studied in air-blast environments owing to their hazardous nature [2,3]. However, in confined explosion scenarios, environmental factors, such as the compartment geometry, crucially impact the dynamics of explosion loading [4,5]. The detonation of fuel-rich explosives disperses numerous unreacted detonation products. Upon exposure to oxygen, these products (particularly CO and carbon) undergo further reactions, releasing additional energy and enhancing the initial blast impact, in a phenomenon referred to as the afterburning effect [6–8].

In open-field explosions, the scaled distance $Z = R/W^{1/3}$ [9], where R represents the stand-off distance and W denotes the charge weight, is a critical parameter that is

extensively used to characterize explosive loading [10–12]. However, confined explosions are substantially influenced by environmental conditions, including the spatial dimensions and extent of enclosure, which significantly alter their dynamics. These explosions typically undergo two distinct phases [13–15]. Initially, they resemble the instantaneous pulse load of open-field explosions, but are characterized by multiple peaks resulting from reflections within the enclosed space. This is followed by a second phase where the dynamics stabilize into a sustained pressure load, referred to as the quasi-static pressure load. Furthermore, the constraints imposed by the confined space can considerably increase the intensity of the explosion, making it several times more powerful than a free-field explosion [16,17]. These differences render the scaled distance Z less effective for describing confined explosive scenarios. Consequently, researchers have proposed replacing the stand-off distance R with the confined space volume V, suggesting W/V as a new characteristic parameter for confined explosions [18]. The choice of V as a parameter is justified by its direct relation to the available oxygen, which influences the extent of combustion of the detonation products [19]. Empirical formulas related to confined explosive loading using the W/V ratio have been derived from experimental data [20–22]. Consequently, manipulating the oxygen content within confined spaces has become the primary experimental approach for studying afterburning effects [23]. Studies [23–25] have indicated that substituting air with inert gases, such as helium and nitrogen, can greatly reduce the intensity of confined explosions, with structural deformations reduced by more than 40% in

scenarios where afterburning is suppressed. Moreover, introducing water mist greatly curtails the afterburning effect, although the underlying mechanisms vary [26]. Further research has shown that the combustion of detonation products is influenced primarily by turbulence caused by wall reflections, as revealed by the expansion rates of fireballs in different gaseous environments [27]. The disparity in propagation speeds between detonation products and shock waves also suggests that afterburning minimally affects the initial shock wave [7].

Theoretical analyses and numerical simulations are crucial for examining blast loading from fuel-rich explosives in confined settings. Edri developed a model to predict the quasi-static pressure in such scenarios, which is based on the thermodynamic properties of detonation products [28,29]. However, this model does not consider the combustion of the detonation products and estimates the quasi-static pressure solely from their final state. Furthermore, the Jones–Wilkins–Lee equation of state has been augmented by incorporating additional energy terms. These modifications have improved the accuracy of modeling post-detonation energy release during afterburning processes, making the computational approach directly applicable in popular commercial solvers such as Autodyn and LS-DYNA [30]. This method depends heavily on precisely defining input parameters regarding the rate and quantity of energy release, necessitating extensive experimental calibration. Therefore, the rational introduction and simplification of these key parameters have attracted considerable attention [31,32]. In the realm of gas explosions, scholars have employed computational fluid dynamics

to investigate gas and dust explosions [33–36], analyzing them as reactive fluids. This approach effectively accounts for the combustion of various components under pressure loading. However, no similar in-depth studies have been conducted on fuel-rich explosives [37]. The scarcity of detailed data on the pressure load histories of confined explosions has fundamentally limited advanced research in this area.

Extant research highlights that the blast loading of fuel-rich explosives in confined spaces remains inadequately explored. Generally, these loadings are managed through simplified rates of energy release in numerical simulations [29] or are based on final-state analyses in theoretical studies [28]. The few studies that have accounted for chemical reaction mechanisms have failed to achieve effective validation against experimental data, and no related research has been pursued further [8]. Both numerical and theoretical frameworks fall short in accurately representing the combustion behaviors of detonation products, thereby impeding an understanding of afterburning effects on explosive loading during such events. The common problem lies in the insufficient comparative validation between experiments and numerical simulations, which has resulted in the lack of a standardized method applicable to confined explosions of various fuel-rich explosives. To address this problem, we designed and executed experiments using $C_7H_5N_3O_6$ (TNT) in a confined space to analyze the energy release characteristics of fuel-rich explosives. TNT is classified as a highly negative oxygen balance explosive with an oxygen balance rate of -74.0%. This indicates that the available oxygen in TNT is insufficient to completely oxidize the other combustible

elements, causing the release of a substantial amount of combustible material as detonation products during an explosion. Additionally, we developed a model that incorporates the combustion of detonation products as a reactive flow component. The model was validated against experimental results, shedding light on the energy release behavior of fuel-rich explosives in confined environments. This study aims to provide data support and analytical methods to facilitate a deeper understanding of the confined explosion behavior of fuel-rich explosives and lay the groundwork for the further exploration of explosion behavior in more complex environments.

2. Experimental method

Based on the volumetric composition of atmospheric oxygen (21% O_2), stoichiometric analysis indicates that the complete oxidation of 1 mol of TNT requires 0.591 m^3 of air. When scaled to the unit mass, the critical confinement volume for the full combustion of 1 kg of TNT is calculated as 2.584 m^3. This establishes a threshold W/V ratio of 0.387 kg/m^3, below which sufficient oxygen is available in a confined system to sustain complete reactions of the detonation products under idealized conditions. Consequently, below this critical ratio, oxygen-rich environments demonstrate enhanced afterburning effects during confined TNT explosions.

As depicted in Fig. 1, a confined chamber was designed with a hollow structure, featuring open ends, internal dimensions of 900 mm × 400 mm × 400 mm, and a wall thickness of 20 mm. For the experiments, target steel plates were sealed at both ends to create a controlled explosive environment with 20 mm-thick flanges. The explosive

charge was centrally suspended and initiated with a detonator. The internal pressure and temperature were monitored using a PCB CA102B pressure sensor and C2-7-K-L thermocouple temperature sensor, respectively, which were placed as depicted in Fig. 1. The data acquisition system used for measuring the load data was operated at a sampling frequency of 10^6 Hz. The CA102B pressure sensor, equipped with an ablation-resistant coating on its sensing surface, reliably captures data under instantaneous shocks at up to 1500 °C. The C2-7-K-L thermocouple, with a response time of 20 ms, accurately measures temperatures up to 1300 °C.

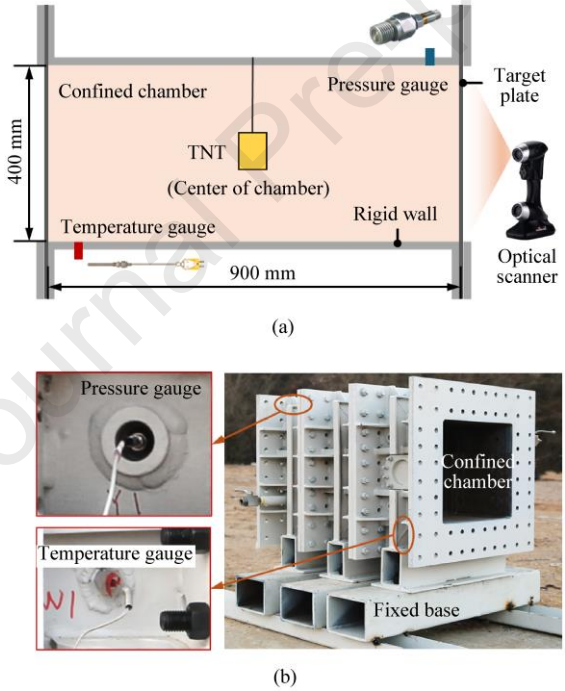

Fig. 1. Confined explosion setup: (a) Test layout; (b) Arrangement of pressure and temperature gauges.

To investigate the afterburning characteristics of the fuel-rich explosives, we conducted experiments using three different charge masses in the confined chamber. Considering the chamber dimensions of 900 mm × 400 mm × 400 mm, the charge mass

required to achieve noticeable afterburning effects was less than 56 g. The TNT charges, which were cylindrical, were detonated at one end using a detonator. The explosives used in the test were obtained from the Beijing Institute of Technology, with a detonator equivalent of approximately 1 g of TNT. Following each test, any residual material was meticulously removed from the chamber to avoid any interference with subsequent experiments. The chamber was sealed with 2.7 mm-thick target plates, each with a tensile strength of 364 MPa. The deformation contours of the target plates were captured using an optical scanner, which provided valuable insights into the structural impacts of the explosions.

3. Numerical simulations

3.1. Afterburning model considering the combustion of detonation products

The reaction fluid is governed by the continuity, momentum, and energy equations. A chemical reaction source term added to the energy equation describes the energy release of the detonation products [8], and the Arrhenius equation describes the energy release mechanism of the chemical reaction source term [36]. Chemical kinetics examines the reaction mechanisms and rates at which chemical species interact at the molecular level. In the context of modeling the transport of reactive species, the reaction rates k for all reactions in the chemical mechanism serve as source terms for the transport equations. These rate constants are typically determined using the Arrhenius equation, which describes the rate as a nonlinear function of the temperature:

$$k = AT^{\beta} \exp\left(-\frac{E_a}{R_u T}\right) \tag{1}$$

where R_u denotes the universal gas constant, A denotes the pre-exponential factor, β is the temperature index, and E_a represents the activation energy.

In the model of reactive transport, all species are subject to convection and diffusion across the computational domain and engage in chemical reactions according to the established reaction mechanism. This study employs the Eddy Break-Up (EBU) model to simulate the dynamics of reactive fluids. In this model, the reaction rate is influenced by the achievable rates of turbulence, as well as the mixing of reactants and thermal energy.

To analyze practical scenarios in a confined explosion setting involving fuel-rich explosives, the key processes, initial pressure, and initial temperature must be clarified. The explosion of fuel-rich explosives typically comprises three stages [36]: (1) Detonation stage: During this stage, the detonation wave propagates through the explosive material, generating detonation products. This stage generally lasts several microseconds. (2) Adiabatic expansion stage: Oxygen does not participate in the reaction during this phase, which usually persists for hundreds of microseconds. (3) Afterburning stage: In this final stage, the detonation products mix with oxygen, combust, and release additional energy. The dynamics of the explosion process for TNT explosives in a confined environment are depicted in Fig. 2.

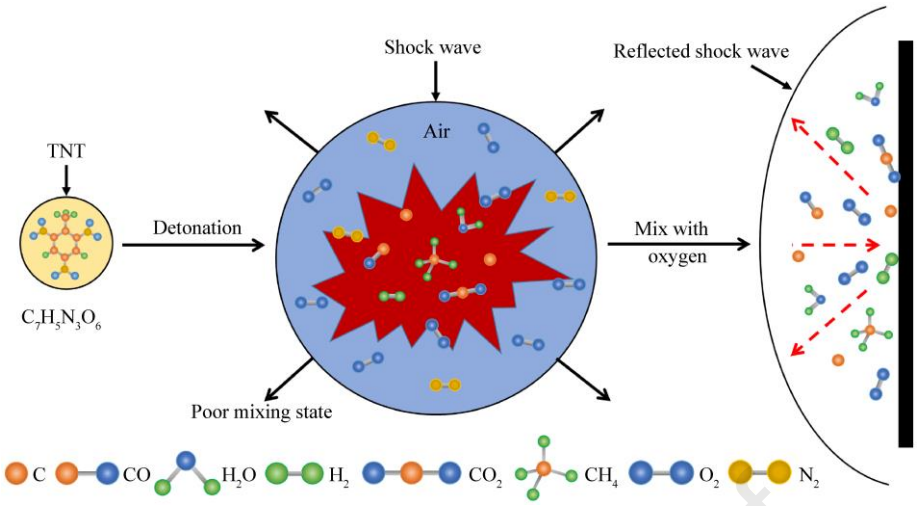

Fig. 2. Explosion dynamics of TNT in a confined space.

The TNT explosion within a confined space was numerically simulated to mirror the actual explosive process through three distinct stages: (1) the detonation stage, where the explosion is assumed to be an instantaneous detonation [38,39]; (2) the adiabatic expansion stage, characterized by the minimal mixing of air with the detonation products, indicating suboptimal mixing conditions under which little energy is released from the detonation products; and (3) the afterburning stage, where the reflected shock wave enhances the mixing of the detonation products with oxygen.

During detonation, CO, H_2, CH_4, and carbon—all combustible—release additional energy when they are sufficiently mixed with oxygen in a high-temperature environment. Thermodynamic polynomial data were utilized to accurately model the gases. Specifically, the heat capacity (C_p) of the gaseous products was characterized using a polynomial equation with five coefficients, effectively capturing the behaviors of these gases under various conditions.

$$\frac{C_p}{R} = a_1 + a_2 T + a_3 T^2 + a_4 T^3 + a_5 T^4 \quad (2)$$

The primary detonation products involved in the afterburning process of a TNT explosion include CO, H_2O, N_2, CO_2, H_2, CH_4, and carbon [40]:

$$C_7H_5N_3O_6 \rightarrow 2.2CO + 1.6H_2O + 1.5N_2 + 1.1CO_2 + 0.36H_2 + 0.27CH_4 + 3.43C \quad (3)$$

The composition was derived from Cheetah equilibrium analysis, which focuses solely on the primary species and ensures the balance of the reaction equation by normalizing the Cheetah values. Additionally, atmospheric N_2 and O_2 play crucial roles. The heat capacities of these substances at specific temperatures were determined using polynomial coefficients [39], as depicted in Fig. 3(a). Because the detonation in this study occurred under constant-volume conditions, the heat capacity at constant volume (C_v) was calculated. The relationship between the heat capacity at a constant pressure (C_p) and the heat capacity at a constant volume (C_v) can be expressed using the following equation:

$$C_p - C_v = R \quad (4)$$

Furthermore, the C_v values for the various substances were obtained, as shown in Fig. 3(b).

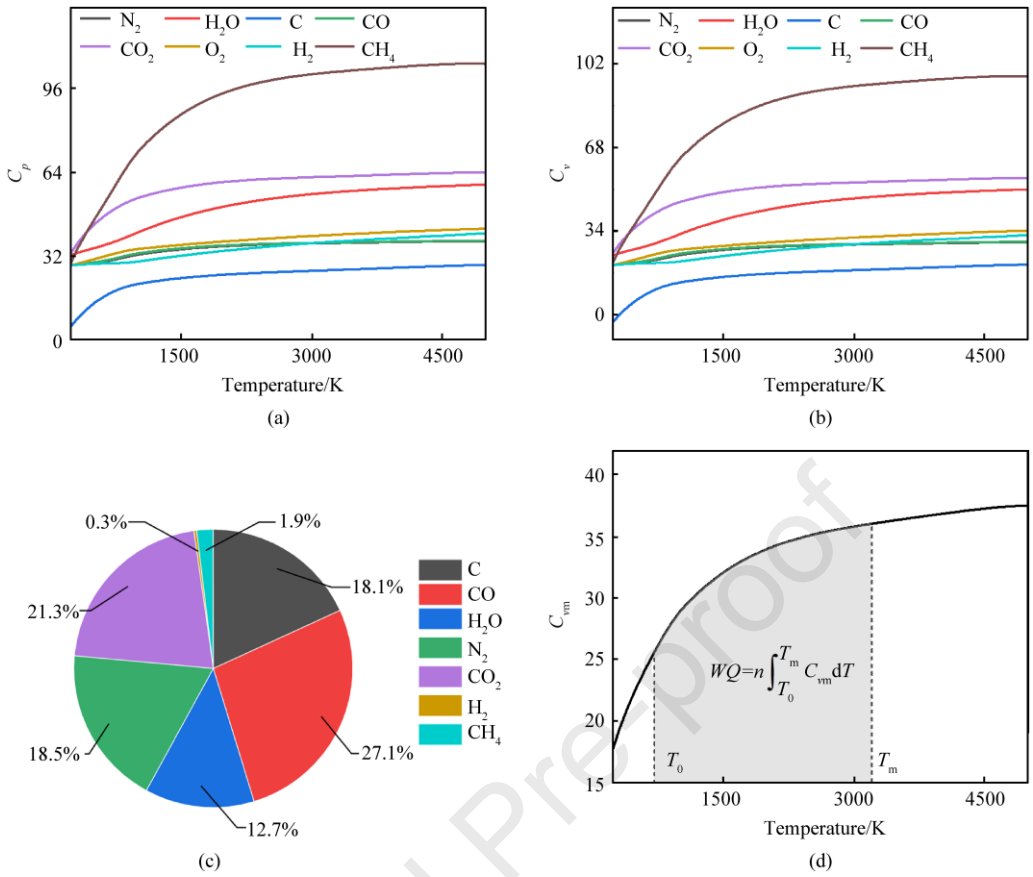

Fig. 3. Key parameters: (a) Heat capacity of the reactive fluid components at a constant pressure (C_p); (b) Heat capacity of the reactive fluid components at a constant volume (C_v); (c) Mass fraction of the detonation product; (d) Thermodynamic relationships.

The temperature T_m of the mixed gases within the high-pressure gas can be obtained using thermodynamic relationships.

$$WQ = n\int_{T_0}^{T_m} C_v \mathrm{d}T \tag{5}$$

where C_v represents a temperature-dependent function. Eq. (5) indicates that the energy WQ required to increase the temperature of n moles of gas from T_0 to T_m can be determined using C_v. Given WQ, n, C_v, and T_0, the initial temperature T_m of the high-pressure gas was determined.

The mass-weighted heat capacity at a constant volume (C_{vm}) of the mixed gases is computed as follows:

$$C_{vm} = \sum_{i=1}^{N} y_i C_v(i) \tag{6}$$

where y_i and $C_v(i)$ represent the mass fraction and heat capacity at a constant volume of component i of the mixed gases, respectively, with N indicating the total number of components in the mixture.

The mass fractions of the detonation products in the mixed gases are detailed in Fig. 3(c). For explosives with specific compositions, such as TNT, the detonation products are assumed to remain relatively stable, enabling the initial pressure and temperature to remain constant across different charge masses when the explosive is converted into a high-pressure gas of equal volume. In the case of a 28 g TNT explosion, the total substance produced by the detonation was 1.2895 mol. With an initial temperature T_0 of 298 K and a specific detonation energy of 4.495 MJ/kg, the initial temperature of the detonation products was calculated to be 3366 K using the integrated C_{vm} function illustrated in Fig. 3(d). By employing the ideal gas law to define the initial state of the high-pressure gas, the initial pressure p_0 can be formulated as

$$p_0 = \frac{nRT_0}{V} \tag{7}$$

where n indicates the total amount of detonation products, R denotes the ideal gas constant, and V denotes the volume of the explosive charge. Given the parameters associated with the TNT detonation process, the initial pressure of the high-pressure

gas was determined to be 2016 MPa. Notably, this methodology for determining the initial parameters is applicable to any explosive scenario with known detonation products and energy values. Fig. 4 depicts an afterburning model for fuel-rich explosives in a confined space based on reactive flow dynamics.

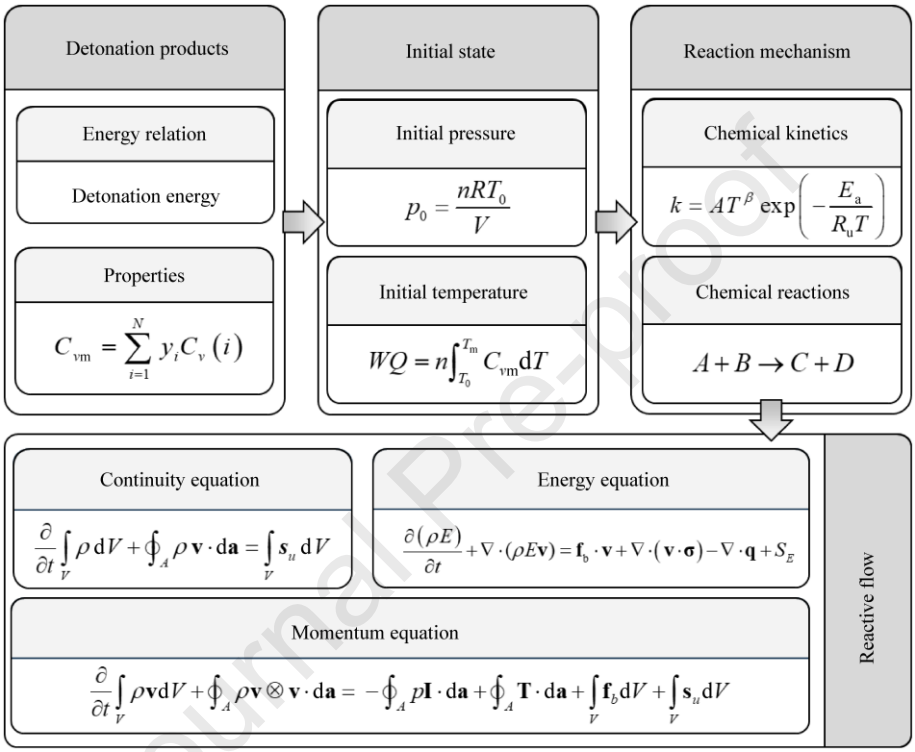

Fig. 4. Afterburning model for fuel-rich explosives based on reactive flow dynamics.

3.2. Numerical model for confined explosions

The afterburning model was employed to develop a numerical model that simulates a blast environment within a confined space. The model represents a confined chamber with dimensions of 900 mm × 400 mm × 400 mm within the fluid domain, starting with an initial temperature of 298 K and initial pressure of 0.1 MPa. The high-pressure gas with an initial temperature of 3366 K and a pressure of 2016 MPa fills the actual volume of the explosive charge. Additionally, specific gas compositions were

assigned based on the proportions of different gases in the fluid domain. Notably, the mass fractions of nitrogen and oxygen in the air domain were 0.767 and 0.233, respectively. While the initial conditions remained consistent across different charge sizes, the volume of the high-pressure gas varied correspondingly. In addition, the potential chemical reactions of the detonation products had to be defined. This study considered only a simplified chemical reaction process, deliberately excluding complex reversible reactions. The primary chemical reactions, as presented in Table 1, were characterized by their corresponding reaction rate coefficients [41].

Table 1

Chemical reaction parameters of the detonation products.

Detonation products	Chemical reaction	Pre-exponential factor	Activation energy /(J·mol^{-1})
C	$C + O_2 \rightarrow CO_2$	1.0×10^{15}	1.0×10^{5}
CO	$CO + 0.5O_2 \rightarrow CO_2$	7.0×10^{7}	6.7×10^{4}
H_2	$H_2 + 0.5O_2 \rightarrow H_2O$	4.0×10^{14}	6.7×10^{4}
CH_4	$CH_4 + 2O_2 \rightarrow CO_2 + 2H_2O$	1.6×10^{13}	1.1×10^{5}

The combustion of the detonation products was simulated using the EBU model within Simcenter STAR-CCM+. The realizable *k*-epsilon turbulence model was utilized to address the interactions between the detonation products and surrounding air. Owing to the temperature-dependent characteristics of chemical reactions, which are influenced by the mixing efficiency and oxygen availability, an adaptive mesh refinement (AMR) strategy was employed. This strategy featured a minimum grid size

of 1 mm to enhance the computational efficiency. The criteria for mesh adaptation, governed by the concentrations of detonation products and temperature gradients, adopted a midpoint subdivision approach to accurately delineate reaction fronts, thereby reducing computational overhead during the initial stages. The confined explosion model, as depicted in Fig. 5, utilized 64-core parallel processing at 4.1 GHz to achieve a temporal resolution of 5 ms within 120 computing hours.

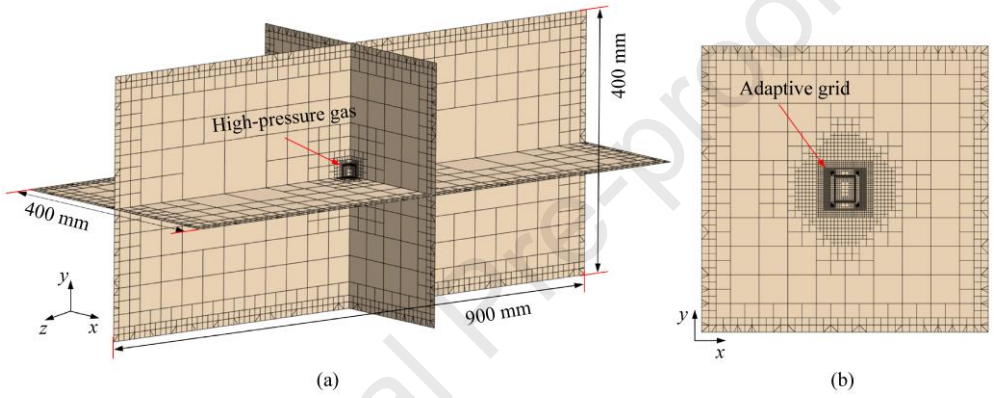

Fig. 5. Numerical model for confined explosions: (a) Computational fluid dynamics model; (b) AMR update.

4. Results and discussion

4.1. Explosive loading in confined spaces

The temperature and pressure load histories recorded during the experiment are shown in Fig. 6. In Fig. 6(a), the temperature clearly shows a pattern of rapid increase followed by a gradual decrease. Although real-time temperature measurements at the gauge points were not feasible, the pattern indicates that temperature conduction occurred much slower than pressure evolution. This observation suggests that the initial stages of the explosion within the confined chamber were adiabatic, allowing for the

assumption that the energy released by the charge explosion was entirely converted into the internal energy of the mixed gases. The pressure histories under various charge conditions are shown in Figs. 6(b)–6(d).

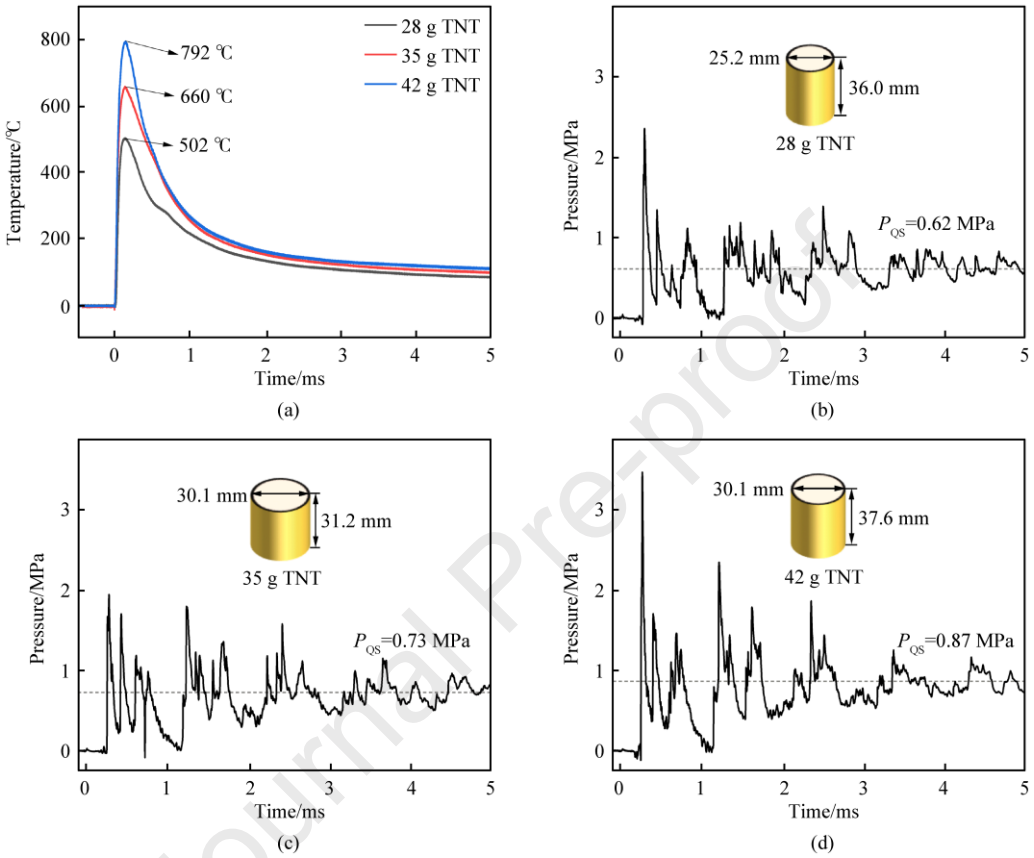

Fig. 6. Loading characteristics from explosive tests: (a) Temperature histories; (b) Pressure histories for 28 g of TNT; (c) Pressure histories for 35 g of TNT; (d) Pressure histories for 42 g of TNT.

Despite efforts to contain the high-pressure gas, leaks through the clamping gaps and bolt holes in the target plate were observed, as depicted in Fig. 7(a). This noticeably decreased the pressure, indicating that the detonation products could not fully undergo combustion reactions. The pressure trends over an extended duration, primarily analyzed based on the pressure data recorded within the first 5 ms of the explosion, are

shown in Fig. 7(b). During this period, a stable quasi-static pressure was noted, with no significant trends of pressure decrease observed.

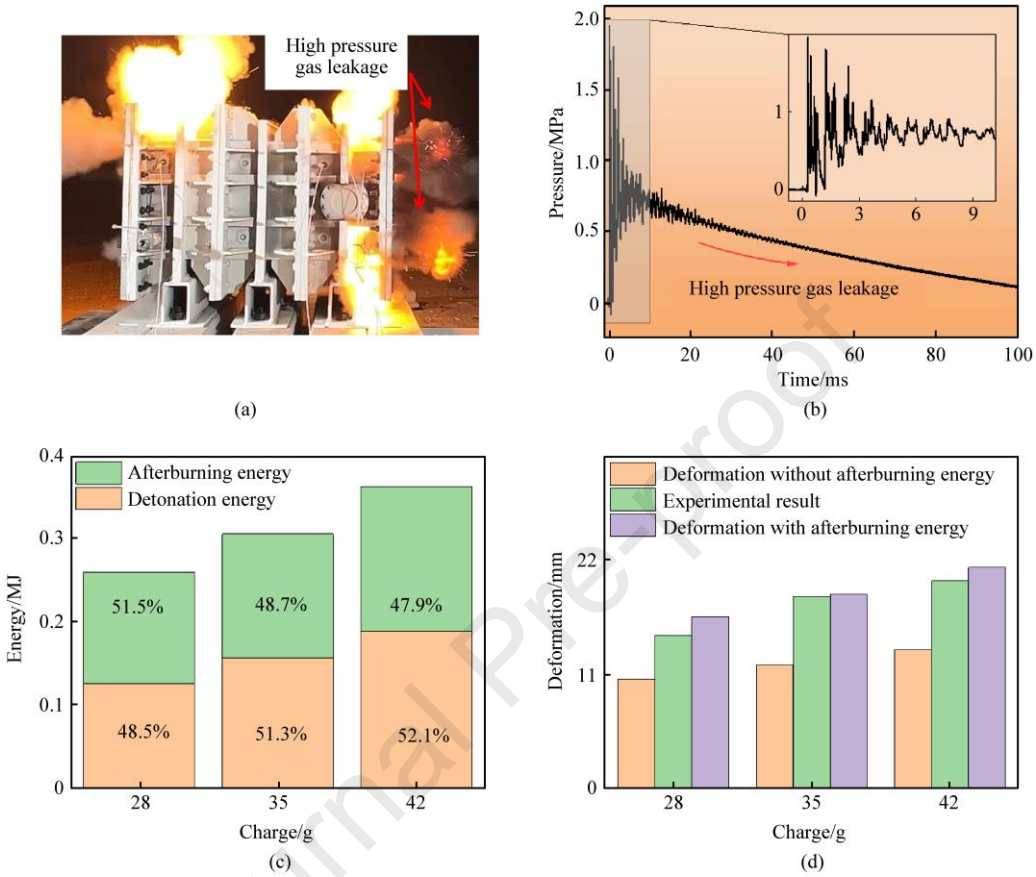

Fig. 7. Confined explosion dynamics: (a) Leakage of high-pressure gas; (b) Extended pressure histories; (c) Energy relationships at various charge levels; (d) Estimation of target plate deformation based on the input energy.

The detonation energy of TNT predicted by Cheetah was 4.495 MJ/kg, and the total energy released from the complete combustion of all the products was 10.01 MJ/kg [29]. This indicates that the total energy was 3.23 times the original detonation energy when the full potential of the detonation products is considered. Theoretically, when the complete release of afterburning energy is considered, this afterburning component constitutes 69% of the total released energy.

Assuming that the volume of the explosive charge is negligible compared with the volume of the confined space [29],

$$Q = \left(\frac{p_{\mathrm{m}}}{\gamma_{\mathrm{m}} - 1} - \frac{p_0}{\gamma_0 - 1} \right) \Big/ \frac{W}{V} \tag{8}$$

The total energy Q released in a confined environment can be estimated through quasi-static pressure measurements, coupled with the relatively stable detonation energy. The energy released from the afterburning phase during the explosion process can thus be calculated. The results detailed in Fig. 7(c) show that as the charge amount increases, the proportion of afterburning energy to the total released energy gradually decreases but always remains below the theoretical maximum of 69%. This suggests that in a confined space, despite ample oxygen to support the combustion of the detonation products, the actual energy released does not reach the ideal level. This shortfall is primarily due to factors such as temperature changes in the detonation products during diffusion and their degree of mixing with oxygen. Essentially, combustible detonation products release their full energy only under optimal conditions, which include the precise temperature settings and appropriate fuel–oxygen mixing required for chemical reactions. Simultaneously, during the initial stages, when the detonation products and air are not thoroughly mixed, the expansion of these products can cause air leakage through gaps in the device. This leakage reduces the amount of air available for reactions, subsequently leading to afterburning energy levels that are below the theoretical maximum. However, the proportion of afterburning energy in the

total energy released is approximately 50%. The addition of this significant amount of energy substantially influences the load histories and represents a critical factor, meriting further investigation of its impact on the structural responses.

4.2. Dynamic response of the target plate

The deformation contours of the target plates after testing were captured using an optical scanner, revealing central deformations of 14.7, 18.4, and 19.9 mm. The deformation exhibited a pronounced dome shape with clear plastic hinges extending diagonally toward the edges.

To quantify the response of the target plate in a confined space explosion scenario, the dimensionless response number ϕ_{in} was introduced [42]:

$$\phi_{in} = \frac{E_e V_e}{\sigma_0 \left(LL_b\right)^{1/2} H^2} \tag{9}$$

where E_e represents the explosive energy per unit volume, V_e represents the explosive volume, σ_0 denotes the material strength, L denotes the length of the target plate, L_b denotes the length of the cuboid chamber, and H denotes the thickness of the target plate.

Moreover, a linear relationship exists between the dimensionless number ϕ_{in} and dimensionless deformation δ/H,

$$\delta/H = 0.0178\phi_{in} + 0.7678 \tag{10}$$

The predicted dimensionless deformation falls within a narrow interval of ±1 δ/H, demonstrating good prediction accuracy. Notably, the dimensionless number ϕ_{in} is

derived by excluding afterburning effects; thus, it accounts only for the detonation energy and does not consider the additional energy input from afterburning. By incorporating an expected deviation of +1 δ/H, the predicted deformation for the test conditions can be determined, as shown in Fig. 7(d). Predictions omitting afterburning effects were generally found to be 30% lower than actual measurements, highlighting the significant impact of afterburning on the explosive yield in confined explosions.

Furthermore, by incorporating the afterburning energy described in Section 4.1 into the dimensionless response number ϕ_{in}, the predicted values for the target plate deformation were recalculated to account for all input energies. Notably, the predicted deformations surpassed the experimental measurements when all energy inputs were considered. This discrepancy primarily arises from the afterburning energy being released at a rate lower than that of the dynamic response of the structure. Although this energy continues to be released over time, only a portion significantly contributes to the structural deformation. This observation is consistent with the phenomenon of structural saturation under dynamic responses [13].

4.3. Effect of the combustion of detonation products on pressure histories

Three sets of numerical simulations were conducted with charges of 28, 35, and 42 g to evaluate the impact of chemical reactions, and the resulting pressure histories are shown in Fig. 8. Figs. 8(a), 8(c), and 8(e) show the effects of the chemical reactions of the detonation products, whereas the results presented in Figs. 8(b), 8(d), and 8(f) do not consider these reactions. The pressure histories that incorporate the afterburning of

the detonation products are consistent with the experimental data, particularly in capturing the initial pressure peak and subsequent transient changes. The deviations between the quasi-static pressures derived from the numerical simulations and experimental values were 9.8%, 11.0%, and 9.2%, respectively. This discrepancy may be attributed to gas leakage from the testing chamber, although its impact is negligible in the early stages, generally causing the calculated values to exceed the experimental results. The numerical discrepancies in impulses at 1.1 ms compared with the experimental results were 8.7%, 8.8%, and 7.1%, respectively, which were primarily due to slightly lower calculated peak values. As the impulse duration increased, the deviation caused by the initial peak discrepancies decreased, with errors reduced to less than 3% by 3 ms.

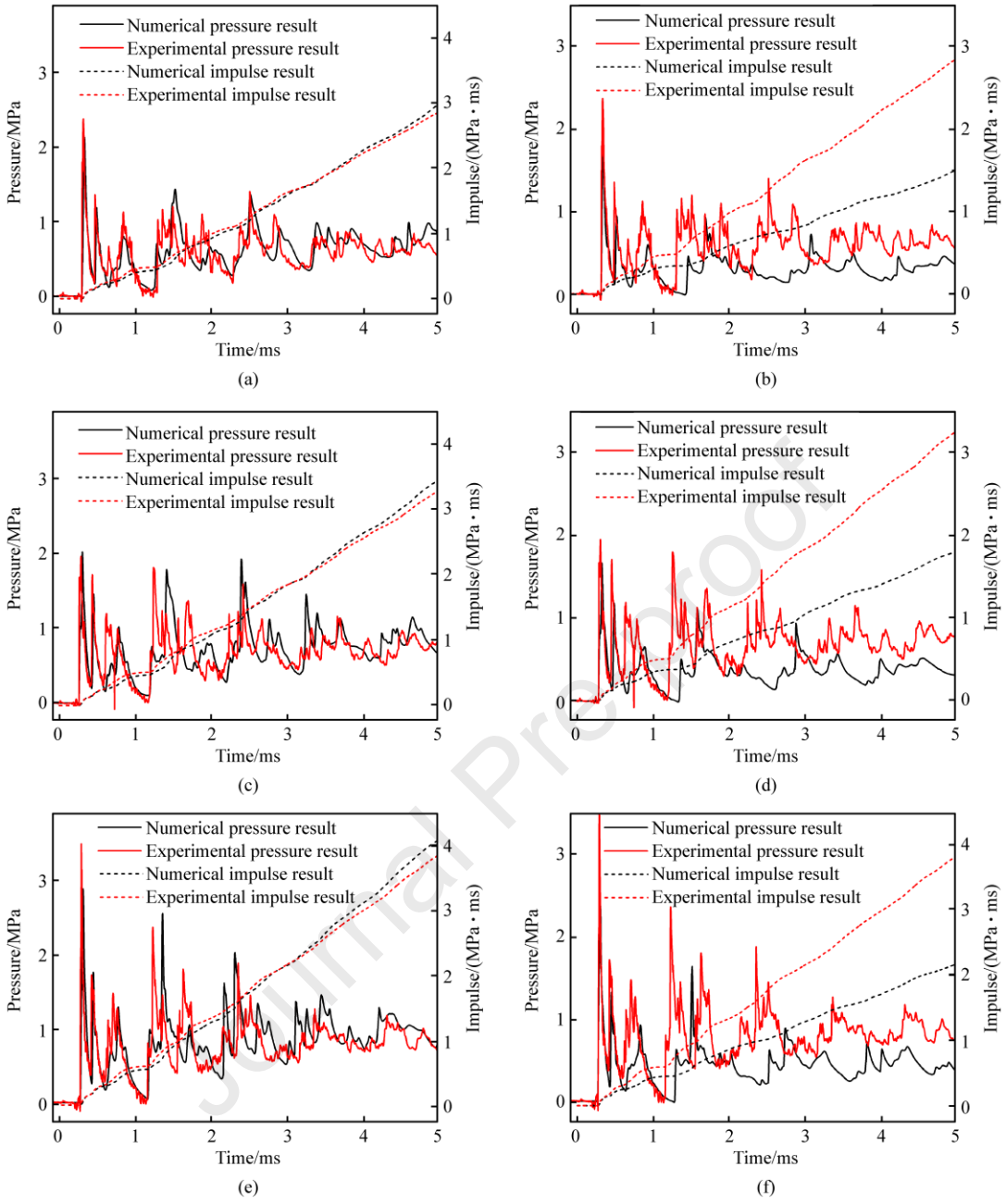

Fig. 8. Comparative analysis of pressure histories: (a) 28 g of TNT with afterburning; (b) 28 g of TNT without afterburning; (c) 35 g of TNT with afterburning; (d) 35 g of TNT without afterburning; (e) 42 g of TNT with afterburning; (f) 42 g of TNT without afterburning.

Notably, the experiments were not conducted in a completely sealed environment, which led to some pressure leakage after the explosion. This leakage reduced the experimental pressure histories after a brief period of quasi-static pressure, which caused the numerical results to exhibit higher impulse values in later stages than the experimental data. Nevertheless, the methodology developed to account for the afterburning of detonation products effectively replicates the real physical environment and provides a robust tool for analyzing explosive loading characteristics in confined spaces.

A further comparison with pressure histories that did not consider the combustion of detonation products, as shown in Figs. 8(b), 8(d), and 8(f), reveals that the difference in the initial peak values is relatively minor, with the impulse difference after the first peak being less than 10%. However, in the experimental setup, the pressure load exhibited a noticeable overall rising trend due to the combustion of detonation products, whereas in the numerical simulations that omitted afterburning, the pressure tended to stabilize more directly. The final quasi-static pressure differences were 45.2%, 46.6%, and 46.0%, respectively. These findings align closely with those reported by Zhou et al. [25], who noted that the quasi-static pressure in a nitrogen environment was 46.9% lower than that in air.

Notably, the aspect ratio of the charge influenced the magnitude of the initial shock wave peak. In the numerical simulations, the pressure peak at the gauge did not increase with increasing charge mass. Instead, it followed a pattern consistent with the

experimental data, where the pressure peak for a 35 g charge was lower than that for a 28 g charge. This trend was observed in both the experimental and numerical results, indicating that changes in the aspect ratio of the charge contribute to variations in the pressure. However, these variations in the initial peak had a minor impact on the subsequent impulse. Over time, the magnitude of the impulse still demonstrated an increasing trend with increasing charge mass.

4.4. Evolution of detonation products

The release of energy and the changes in the quantities of substances emitted from the detonation products within the confined space are shown in Fig. 9. The variations in the pressure and mass fractions of CO and CO_2 during the numerical simulations are shown in Fig. 10. Notably, this study utilized high-temperature, high-pressure gases as substitutes for TNT charges, which do not involve the effects of the location of the initiation point. However, the initial gas retains the geometric shape of the TNT charges before detonation, effectively preserving the characteristics of cylindrical charges during the propagation of shock waves and diffusion of detonation products.

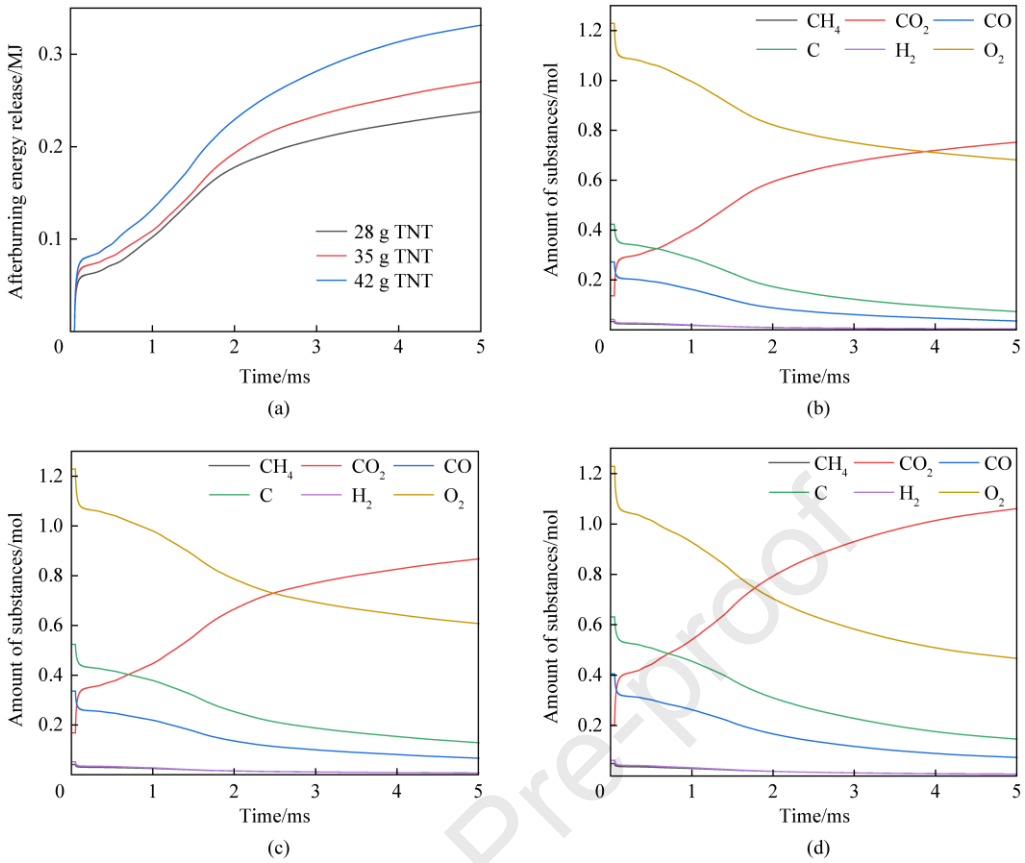

Fig. 9. Analysis of the combustion process in a confined space: (a) Energy release during afterburning; amounts of substance in (b) 28 g of TNT, (c) 35 g of TNT, and (d) 42 g of TNT.

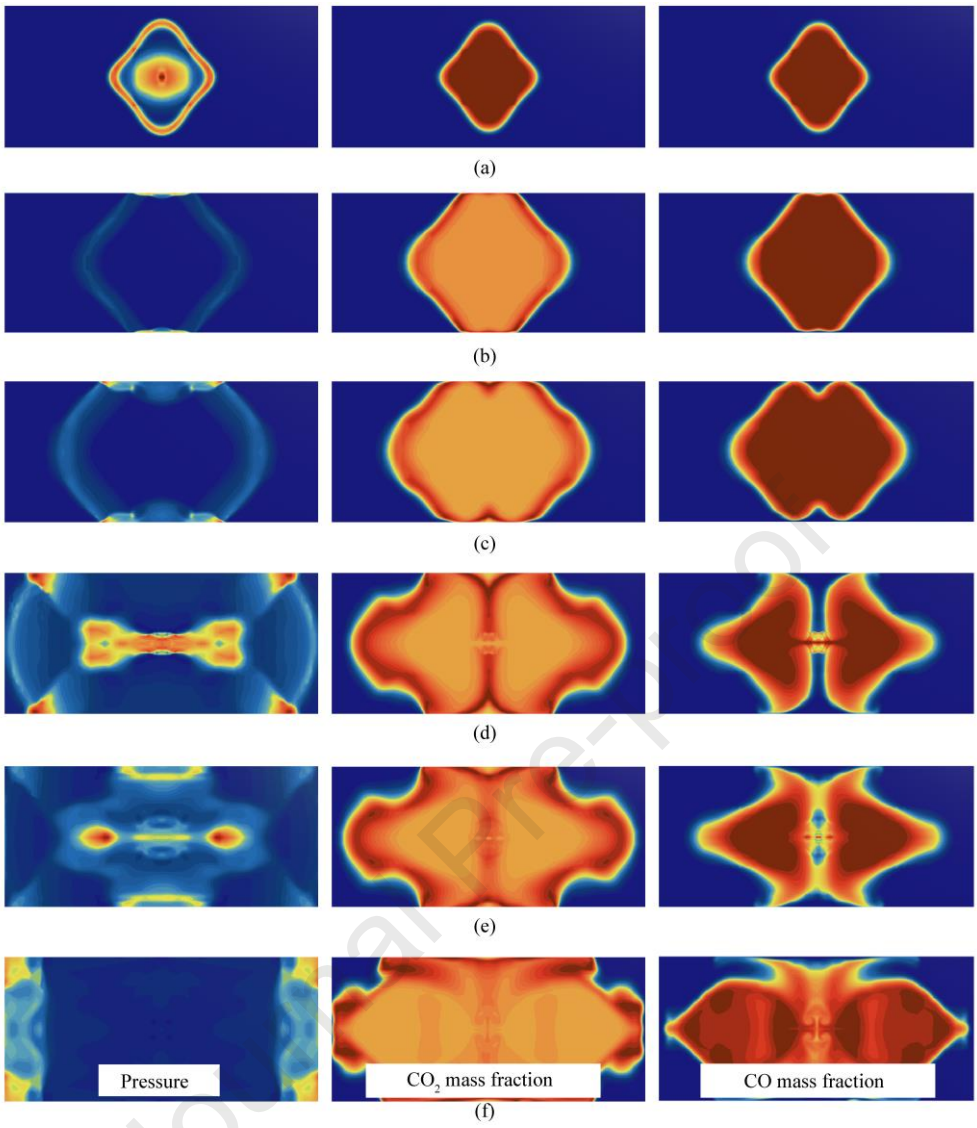

Fig. 10. Evolution of the pressure, CO_2 mass fraction, and CO mass fraction during the explosion of 42 g of TNT: (a) 0.04 ms; (b) 0.08 ms; (c) 0.12 ms; (d) 0.24 ms; (e) 0.28 ms; (f) 0.48 ms.

During the initial 0.05 ms, the detonation products did not undergo chemical reactions. During this period, the total amounts of afterburning energy released and the detonation products remained constant, with the mass fraction distribution contours for CO and CO_2 remaining identical despite the difference in their initial concentrations. The shock wave reached the near wall after 0.05 ms, inducing complex turbulence. At

this stage, the interface between the detonation products and air fulfilled the necessary reaction conditions of temperature and degree of mixing, prompting the detonation products to begin reacting rapidly with oxygen to release energy. This rapid reaction phase lasted approximately 0.1 ms, during which the combustible products at the interface were swiftly consumed. Following their collision with the wall, most of the detonation products were driven into the interior of the high-pressure gas mass. Subsequently, as most of the unreacted detonation products lacked sufficient oxygen, both the quantity of these products and the rate of afterburning energy release decreased noticeably. By approximately 0.3 ms, the detonation products had reached the end walls of the confined chamber and were reflected back, which gradually increased the mixing with oxygen and consequently increased the rate of energy release until approximately 2.0 ms. As the reaction continued, the concentration of combustible components within the confined space gradually diminished, and the reaction of the detonation products also slowed. The energy release during this phase slowed primarily owing to the complex turbulent state that developed inside the confined space, which made the necessary temperature and reactant mixing conditions for sustained chemical reactions increasingly difficult to achieve. The energy release from the detonation products of a 28 g explosive charge ceased after approximately 12 ms, as demonstrated by pressure measurements. These measurements indicated that the afterburning energy contributed between 47.9% and 51.5% of the total energy output. This range is notably below the theoretical maximum of 69%, a discrepancy that can be attributed to two main factors:

(1) pressure attenuation through structural clearances within the experimental setup and (2) incomplete combustion of detonation products owing to the kinetic limitations of the afterburning reactions under time-constrained conditions.

CO_2, a primary product of both TNT detonation and afterburning, initially registered a maximum mass fraction of 0.213. As the afterburning reaction progressed, CO_2 continually formed at the interface, resulting in concentrations higher than its initial mass fraction and creating zones of high CO_2 concentration. This also led to a faster diffusion of CO_2 than of CO. Analyzing the mass fractions of CO and the changes in the pressure load revealed that the diffusion of detonation products greatly lagged behind the propagation of the shock wave. This lag explains why the energy released from the combustion of the detonation products had almost no impact on the initial shock wave load.

In summary, the energy released from the combustion of detonation products in a confined space unfolds into three distinct phases for varying charges, as shown in Fig. 9(a). The energy release rates across these phases differ by almost an order of magnitude. The initial phase features the highest rate of energy release, where the reaction dynamics are predominantly governed by the rates of chemical reactions. Here, the chemical reactions rapidly consume the fuel at the interface between the detonation products and oxygen, producing CO_2 and H_2O. In the second phase, the rate of energy release significantly decreases because of substantial fuel consumption at the interface and the dilution of reactants by CO_2 and H_2O. However, the confined space and the

reflection of shock waves promote more effective mixing of the detonation products with oxygen. The reaction rate during this phase is influenced by the geometric dimensions of the confined space and the distribution of the detonation products, resulting in varying energy release rates for different charges. In the final phase, as the fuel is largely consumed and the reactant concentration becomes diluted, the rate of energy release gradually decreases until the detonation products cease to react and release energy.

4.5. Replicability and applications

4.5.1. Comparison with the JWL equation correction method

A numerical simulation was performed for the experimental conditions in this study using the method proposed in [30]. The modified JWL equation of state was used to model the afterburning effects in a confined explosion scenario. The total afterburning energy, start time, and duration of energy release had to be determined; however, the duration could not be directly determined. Therefore, for the experiments in this study, parametric trial simulations were performed for various durations t_d, and the results are shown in Fig. 11(a).

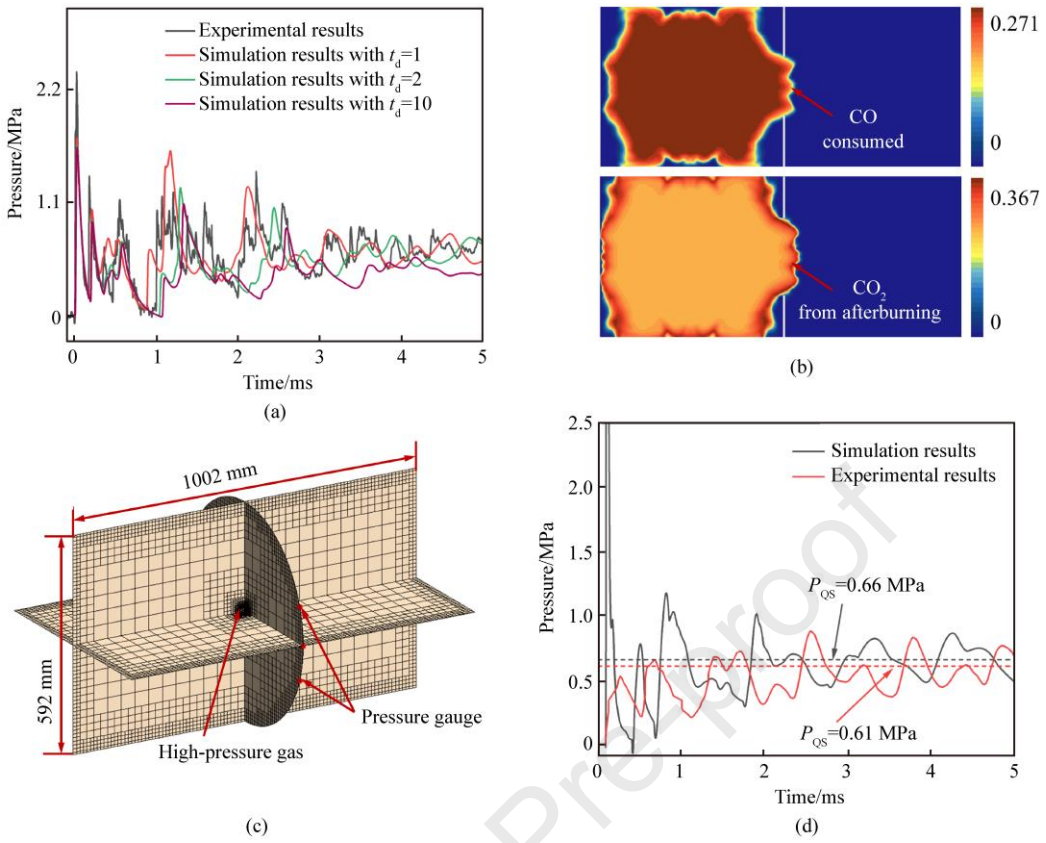

Fig. 11. Comparison and application: (a) Pressure history for various durations; (b) Afterburning in a complex connected space; (c) Numerical computational modeling; (d) Comparison of results.

The results confirm that the method can produce simulation results that are comparable to the experimental results through iterative trial-and-error processes. However, as a critical parameter, the duration is highly dependent on the experimental calibration, and the durations obtained by trial-and-error calculations cannot be generalized. In contrast, the method established in this study relies on the chemical reactions of detonation products to describe the release of afterburning energy. Even simplified chemical reactions can reflect the essential process of afterburning energy

release, thereby eliminating experimental dependence.

4.5.2. Localized connectivity space explosion analysis

In addition, for the 42 g TNT explosion scenario examined in this study, a wall constraint was incorporated into the numerical model, with a 200 mm-diameter vent hole situated in the center to simulate a more intricate space with local connectivity. Clearly, the developed method enables the release of afterburning energy into the adjacent space through the diffusion of detonation products, which cannot be achieved using a traditional method [30]. Conventional methods rely on the fixed oxygen content within the space to determine the amount of afterburning energy released. However, as shown in Fig. 11(b), the diffusion of detonation products, such as CO, through the locally connected region into adjacent spaces, where they come into contact with more oxygen, has been observed. When the detonation products maintain a sufficiently high temperature, they undergo further combustion in the neighboring space, releasing additional energy. This enhanced analytical approach provides a more comprehensive framework for studying the explosive behavior of fuel-rich explosives in complex spaces.

4.5.3. Application to other fuel-rich explosives

To confirm the replicability of the proposed model, a comparative analysis was performed using PE-4 explosives, which exhibited afterburning effects. PE-4 explosives are composed of 87% RDX and 13% mineral oil. Aerobic and anaerobic detonation tests of PE-4 explosives were conducted in a confined cylindrical chamber,

and the pressure history was recorded within the chamber [37]. The detonation products contained combustible components including CO, carbon particles, and small molecular hydrocarbon intermediates. By analyzing the compositional characteristics of the detonation products, the initial temperature and pressure of the high-pressure gas cloud generated during the PE-4 explosion were found to be 3480 K and 1735 MPa, respectively.

A numerical model was established based on the experimental conditions, as shown in Fig. 11(c), and the results for 50 g PE-4 are shown in Fig. 11(d). The experiment was designed to record the quasi-static pressure within a confined space; consequently, the initial overpressure from the simulation is not commensurate with the experimental results. However, the final quasi-static pressure results indicate that the discrepancy between the calculated and experimental results is only 8%, thereby substantiating the efficacy of the method developed in this study in accurately reflecting the explosive behavior of fuel-rich explosives in a confined space.

4.5.4. Discussions

In the context of widely studied open-field explosions, limited research has been conducted on the afterburning process. This is primarily because the reactions at the product–oxygen interface are often hindered by the formation of new products, such as CO_2 and H_2O, which prevent the sustained combustion of detonation products. In open-field scenarios, the focus is predominantly on the initial pressure peak, and as the combustion of detonation products progresses relatively slowly, it has minimal impact

on the outcome of these explosions. However, a confined environment alters the diffusion of the detonation products, resulting in a significantly higher explosive yield for fuel-rich explosives than that observed in an open-field setting. This highlights the importance of considering environmental factors when handling hazardous materials such as fuel-rich explosives. Therefore, the load characteristics observed in open-field tests should not be directly applied to assess the explosive yield in confined spaces, because they do not accurately reflect the dynamics and potential risks associated with such environments.

With frequent terrorist attacks worldwide, confined explosion scenarios, such as inside buildings, underground tunnels, and ship interiors, are becoming increasingly common. The afterburning effects of fuel-rich explosives have a pronounced effect on the intensity of the blast loads. The development of reliable analytical tools for characterizing afterburning effects can improve the understanding of the risks posed by various explosion scenarios and facilitate further refinement of relevant design standards.

5. Conclusions

This study explored the blast-loading characteristics of fuel-rich explosives within confined environments. Experimental investigations were conducted on the detonation of TNT in restricted spaces, and numerical methods that integrate the combustion dynamics of detonation products were subsequently developed. The experimental and computational analyses led to several key conclusions:

(1) In confined spaces, fuel-rich explosives such as TNT exhibit extensive afterburning of detonation products, which is influenced by environmental factors, such as oxygen availability and spatial limitations. The experiments demonstrated that the energy released from the detonation products constituted approximately 50% of the total energy output. Although the burning rate of these products was lower than that of the initial detonation, it matched the dynamic structural response rate, thereby enhancing the overall explosive yield. Neglecting afterburning effects resulted in a reduction of approximately 30% in the center-point deformation of the structure.

(2) A newly developed numerical model incorporating a chemical reaction source term effectively characterizes the loading behavior of fuel-rich explosives in confined environments. This model considers the effects of chemical reactions of the detonation products on the loading dynamics. The inclusion of combustion in the numerical simulations led to a 45% increase in the quasi-static pressure, which aligned with the experimental findings. However, the influence of afterburning on the initial blast loading was minimal, primarily because of the differential diffusion rates between the shock waves and detonation products.

(3) Spatial constraints in confined environments greatly affect the afterburning behavior of detonation products. The experimental setup revealed that the combustion process could be segmented into three distinct phases. Initially, combustion predominantly occurs at the interface between the detonation products and oxygen, governed almost exclusively by the theoretical chemical reaction rate. The subsequent

phases depend on the enclosure dimensions. Once the initial fuel supply at the interface is exhausted, turbulence ensues, facilitating further mixing of the high-pressure gases with oxygen, thereby moderating the rate of detonation product consumption according to the mixing intensity and reaction temperature.

In summary, this study provides detailed experimental pressure history data for TNT explosions in confined spaces and establishes a comprehensive afterburning analysis method based on reactive flow. Further investigations are required to explore mixed explosives, more complex environments, and the applicability of the proposed methods.

Acknowledgments

This work was supported by the National Natural Science Foundation of China (Grant Nos. 52171318 and 12202329) and Joint Foundation of the Ministry of Education (Grant No. 8091B022105).

References

[1] Edri I, Feldgun VR, Karinski YS, Yankelevsky DZ. Afterburning aspects in an internal TNT explosion. Int J Prot Struct 2013;4:97–116. https://doi.org/10.1260/2041-4196.4.1.97.

[2] Xiao W, Andrae M, Gebbeken N. Air blast TNT equivalence concept for blast-resistant design. Int J Mech Sci 2020;185:105871. https://doi.org/10.1016/j.ijmecsci.2020.105871.

[3] Xiao W, Andrae M, Gebbeken N. Air blast TNT equivalence factors of high explosive material PETN for bare charges. J Hazard Mater 2019;377:152–62. https://doi.org/10.1016/j.jhazmat.2019.05.078.

[4] Song S, Cheng Y, Wang W, Wang Z, Zhang B. Explosion behaviors of hybrid

C2H2/CaC2 dust in a confined space. J Hazard Mater 2021;416:125783. https://doi.org/10.1016/j.jhazmat.2021.125783.

[5] Salvado FC, Tavares AJ, Teixeira-Dias F, Cardoso JB. Confined explosions: The effect of compartment geometry. J Loss Prev Proc Ind 2017;48:126–44. https://doi.org/10.1016/j.jlp.2017.04.013.

[6] Kim C, Moon JG, Lai M, In K. Afterburning of TNT Explosive Products in Air with Aluminum Particles. 46th AIAA Aerospace Sciences Meeting and Exhibit, 2008. https://doi.org/10.2514/6.2008-1029.

[7] Balakrishnan K, Menon S. Numerical Investigation of Shear Instability, Mixing and Afterburn Behind Explosive Blast Waves. 47th AIAA Aerospace Sciences Meeting including The New Horizons Forum and Aerospace Exposition, Orlando, Florida: American Institute of Aeronautics and Astronautics; 2009. https://doi.org/10.2514/6.2009-1530.

[8] Balakrishnan K, Menon S. On the role of ambient reactive particles in the mixing and afterburn behind explosive blast waves. Combust Sci Technol 2010;182:186–214. https://doi.org/10.1080/00102200903341579.

[9] Hopkinson B. A method of measuring the pressure produced in the detonation of high, explosives or by the impact of bullets. Phil Trans R Soc Lond A 1914;213:437–56. https://doi.org/10.1098/rsta.1914.0010.

[10] Esparza ED. Blast measurements and equivalency for spherical charges at small scaled distances. Int J Impact Eng 1986;4:23–40. https://doi.org/10.1016/0734-743X(86)90025-4.

[11] Esparza ED, Brode HL. Blast wave from a spherical charge. Phys Fluids 1959;2:217–29. https://doi.org/10.1063/1.1705911.

[12] Edwards DH, Thomas GO, Milne A, Hooper G, Tasker D. Blast wave measurements close to explosive charges. Shock Waves 1992;2:237–43. https://doi.org/10.1007/BF01414759.

[13] Yuan Y, Li X, Zhang C, Tan PJ, Chen P. Impulse saturation in metal plates under

confined blasts. Int J Impact Eng 2022;168:104308. https://doi.org/10.1016/j.ijimpeng.2022.104308.

[14] Yuan Y, Zhang C, Xu Y. Influence of standoff distance on the deformation of square steel plates subjected to internal blast loadings. Thin-Walled Struct 2021;164:107914. https://doi.org/10.1016/j.tws.2021.107914.

[15] Zhang C, Tan PJ, Yuan Y. Confined blast loading of steel plates with and without pre-formed holes. Int J Impact Eng 2022;163:104183. https://doi.org/10.1016/j.ijimpeng.2022.104183.

[16] Geretto C, Chung Kim Yuen S, Nurick GN. An experimental study of the effects of degrees of confinement on the response of square mild steel plates subjected to blast loading. Int J Impact Eng 2015;79:32–44. https://doi.org/10.1016/j.ijimpeng.2014.08.002.

[17] Zhou H, Zheng C, Lu A, Zhu Z, Kong X, Wu W. An experimental study of the effects of degrees of confinement on the response of thermoplastic fibre–metal laminates subjected to blast loading. Thin-Walled Struct 2023;192:111125. https://doi.org/10.1016/j.tws.2023.111125.

[18] Lloyd Register. Rules and Regulations for the Classification of Naval Ships 2022.

[19] Edri I, Feldgun VR, Karinski YS, Yankelevsky DZ. On blast pressure analysis due to a partially confined explosion: III. Afterburning effect. Int J Prot Struct 2012;3:311–31. https://doi.org/10.1260/2041-4196.3.3.311.

[20] Brode HL. Numerical solutions of spherical blast waves. J Appl Phys 1955;26:766–75. https://doi.org/10.1063/1.1722085.

[21] Army tm 5-1300/Navy NAVFAC P-397/Air force AFR 88-22: structures to resist the effects of accidental explosions. Washington DC: Departments of the Army, the Navy, and the Air Force; 1990.

[22] US Army Corps of Engineers. Structures to resist the effects of accidental explosions. 2nd ed. Air Force Civil Engineer Support Agency; 2014. UFC 3-340-02.

[23] Kong X, Wang Z, Kuang Z, Zhou H, Zheng C, Wu W. Experimental study on the mitigation effects of confined-blast loading. Explos Shock Waves 2021;41 :24–37. https://doi.org/10.11883/bzycj-2020-0193.

[24] Kong X, Kuang Z, Zheng C, Wu W. Experimental study of afterburning enhancement effect for blast load in confined compartment space. Acta Armamentarii 2020;41:75–85. https://doi.org/10.3969/j.issn.1000-1093.2020.01.009.

[25] Zhou H, Zheng C, Yue X, Zhu Z, Lu A, Kong X, et al. TNT equivalency method in confined space based on steel plate deformation. Int J Impact Eng 2023;178:104587. https://doi.org/10.1016/j.ijimpeng.2023.104587.

[26] Kong X, Zhou H, Zheng C, Liu H, Wu W, Guan Z, et al. An experimental study on the mitigation effects of fine water mist on confined-blast loading and dynamic response of steel plates. Int J Impact Eng 2019;134:103370. https://doi.org/10.1016/j.ijimpeng.2019.103370.

[27] Tyas A, Reay JJ, Fay SD, Clarke SD, Rigby SE, Warren JA, et al. Experimental studies of the effect of rapid afterburn on shock development of near-field explosions. Int J Prot Struct 2016;7:452–65. https://doi.org/10.1177/2041419616665931.

[28] Edri IE, Grisaro HY, Yankelevsky DZ. TNT equivalency in an internal explosion event. J Hazard Mater 2019;374:248–57. https://doi.org/10.1016/j.jhazmat.2019.04.043.

[29] Feldgun VR, Karinski YS, Edri I, Yankelevsky DZ. Prediction of the quasi-static pressure in confined and partially confined explosions and its application to blast response simulation of flexible structures. Int J Impact Eng 2016;90:46–60. https://doi.org/10.1016/j.ijimpeng.2015.12.001.

[30] Zhou H, Yue X, Zheng C, Zhu Z, Lu A, Kong X, et al. Dynamic behavior of steel plates subjected to confined blast loading considering afterburning effect. Int J Impact Eng 2024;188:104934. https://doi.org/10.1016/j.ijimpeng.2024.104934.

[31] Yue X, Zhou H, Kong X, Zheng C, Wu W. Experimental and simulation study of afterburning effect for blast load in confined cabin. Chin J Ship Res 2023;18:223–32. https://doi.org/10.19693/j.issn.1673-3185. 02708.

[32] Zhou H, Kong X, Zheng C, Wu W. The analysis of the equivalent bare charge of aluminum cased charge exploding in confined space. J Phys: Conf Ser, vol. 1507, Nanjing: IOP Publishing; 2020. https://doi.org/10.1088/1742-6596/1507/3/032008.

[33] Denkevits A, Hoess B. Hybrid H2/Al dust explosions in Siwek sphere. J Loss Prev Proc Ind 2015;36:509–21. https://doi.org/10.1016/j.jlp.2015.03.024.

[34] Redlinger R. Numerical simulation of hybrid dust/gas explosion experiments in the standard 20-L sphere. Fusion Eng Des 2015;100:419–24. https://doi.org/10.1016/j.fusengdes.2015.07.006.

[35] Houim RW, Oran ES. Numerical simulation of dilute and dense layered coal-dust explosions. Proc Combust Inst 2015;35:2083–90. https://doi.org/10.1016/j.proci.2014.06.032.

[36] Zhou Z, Zhao C, Lu C, Le G. Numerical studies on four-engine rocket exhaust plume impinging on flame deflectors with afterburning. Def Technol 2021;17:1207–16. https://doi.org/10.1016/j.dt.2020.06.016.

[37] Farrimond DG, Woolford S, Barr AD, Lodge T, Tyas A, Waddoups R, et al. Experimental studies of confined detonations of plasticized high explosives in inert and reactive atmospheres. Proc R Soc A 2024;480:20240061. https://doi.org/10.1098/rspa.2024.0061.

[38] Xu W, Wu W. An improved third-order weighted essentially non-oscillatory scheme achieving optimal order near critical points. Comput Fluids 2018;162:113–25. https://doi.org/10.1016/j.compfluid.2017.12.010.

[39] Xu W, Wu W, Lin Y. Numerical method and simplified analytical model for predicting the blast load in a partially confined chamber. Comput Math Appl 2018;76:284–314. https://doi.org/10.1016/j.camwa.2018.04.019.

[40] Donahue L, Zhang F, Ripley RC. Numerical models for afterburning of TNT detonation products in air. Shock Waves 2013;23:559–73. https://doi.org/10.1007/s00193-013-0467-2.

[41] Linstrom PJ, Mallard WG. The NIST Chemistry WebBook: A chemical data resource on the internet. J Chem Eng Data 2001;46:1059–63. https://doi.org/10.1021/je000236i.

[42] Zheng C, Wang Y, Kong X, Zhou H, Liu H, Wu W. Predicting the deflection of square plates subjected to fully confined blast loading. J Mar Sci Eng 2020;8:1031. https://doi.org/10.3390/jmse8121031.

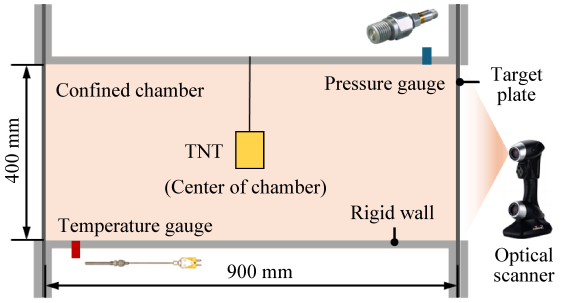

(a)

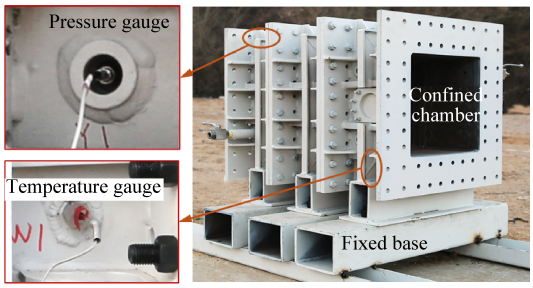

(b)

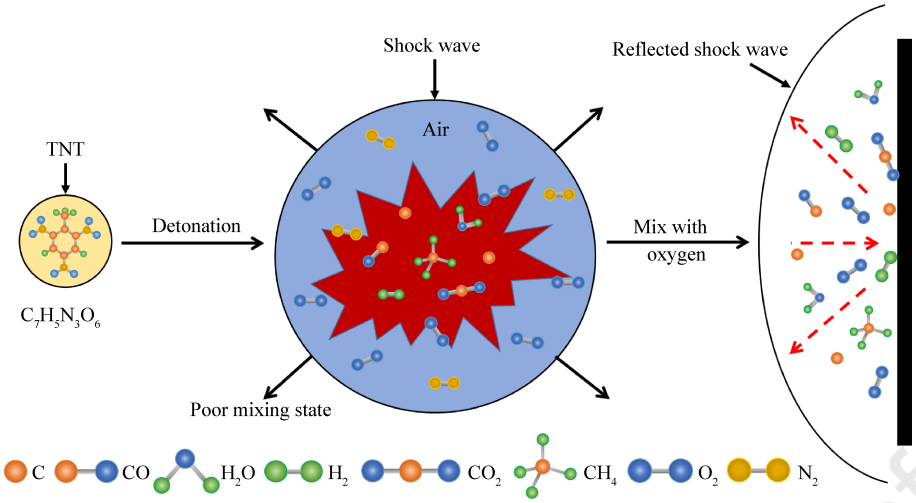

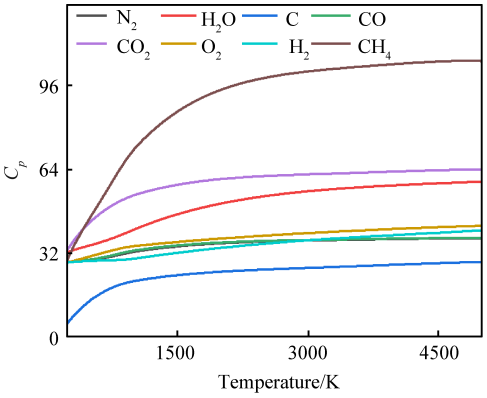

(a)

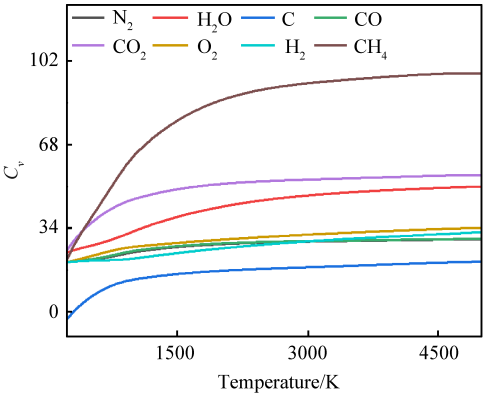

(b)

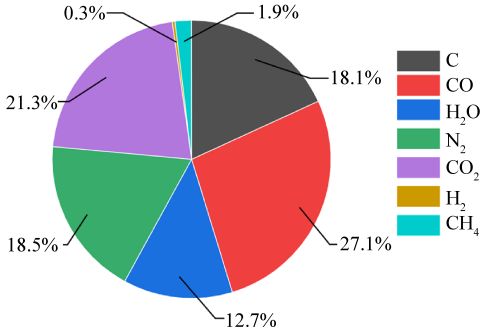

(c)

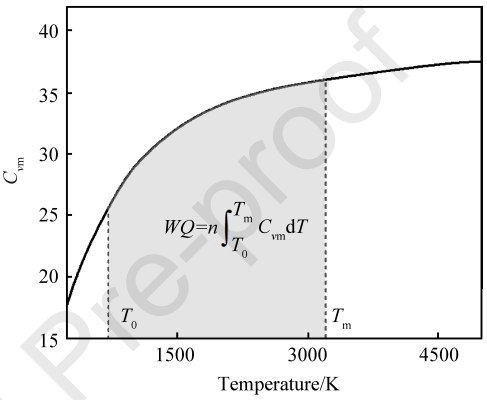

(d)

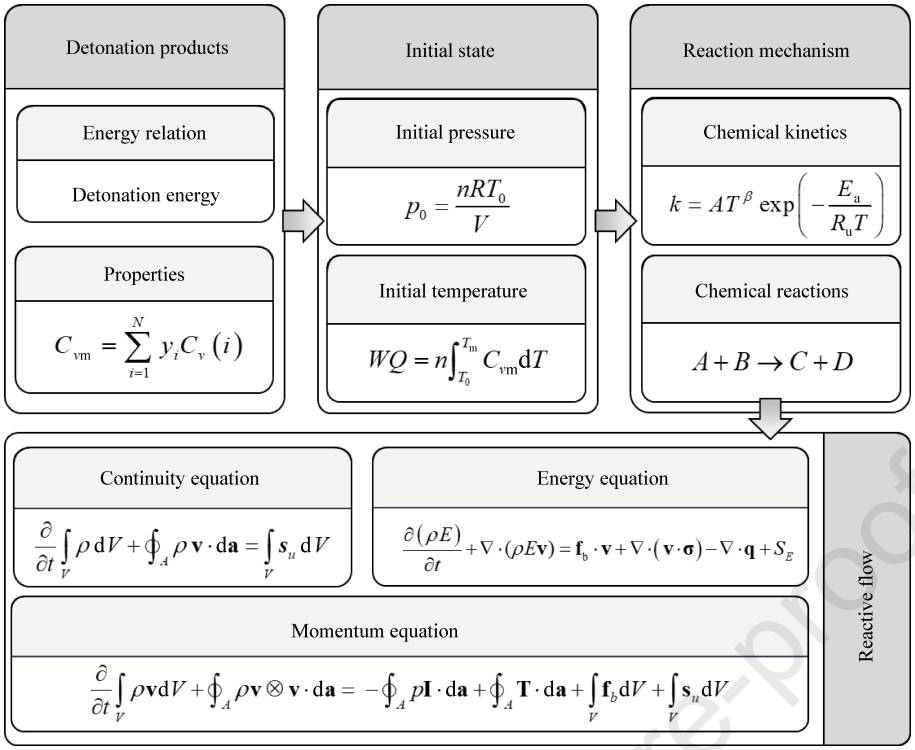

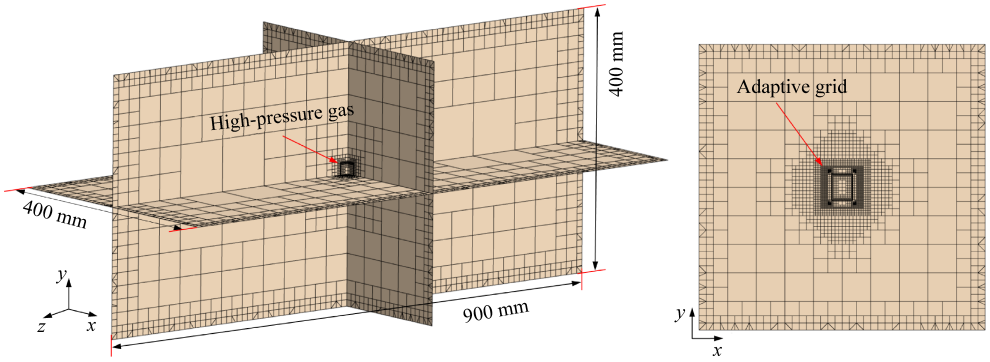

(a) (b)

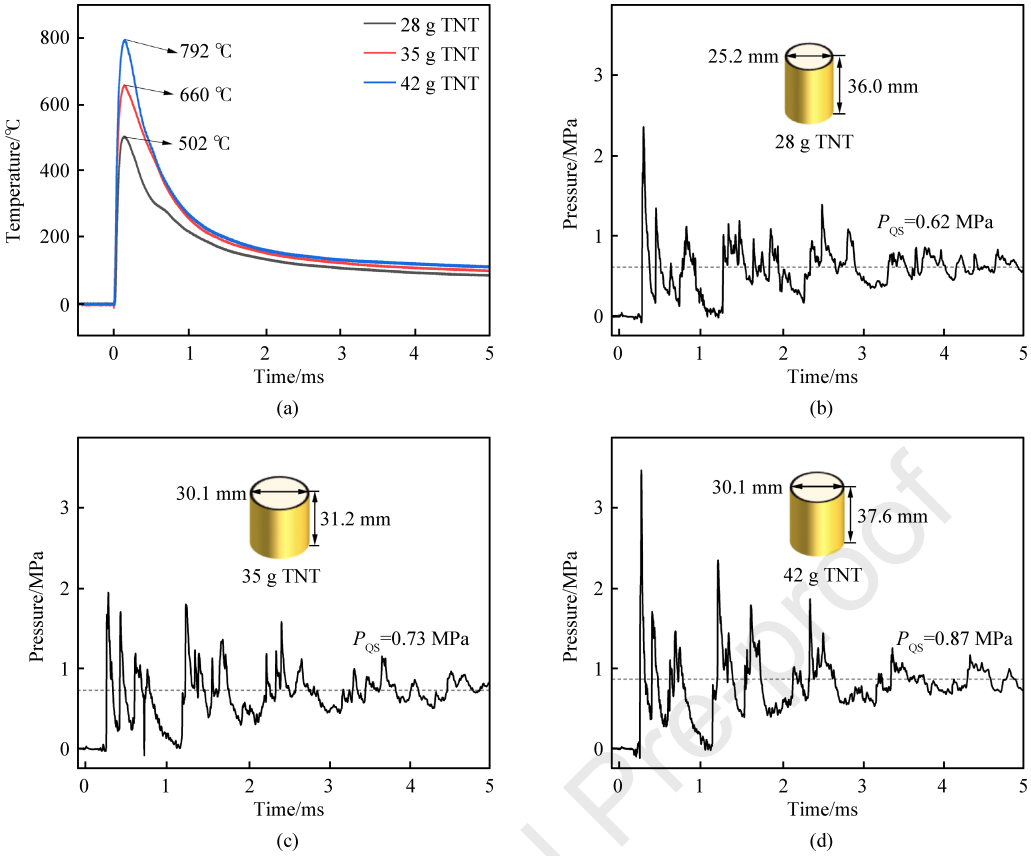

(a)

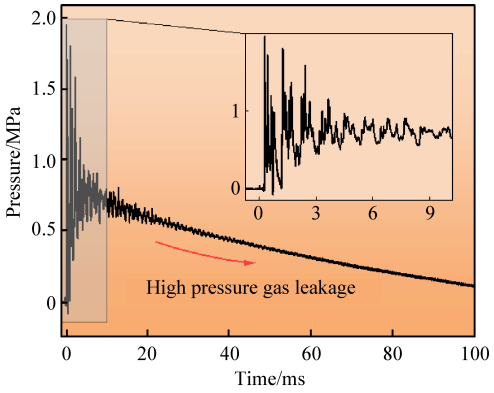

(b)

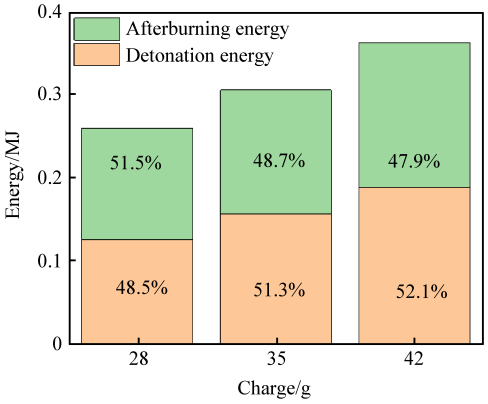

(c)

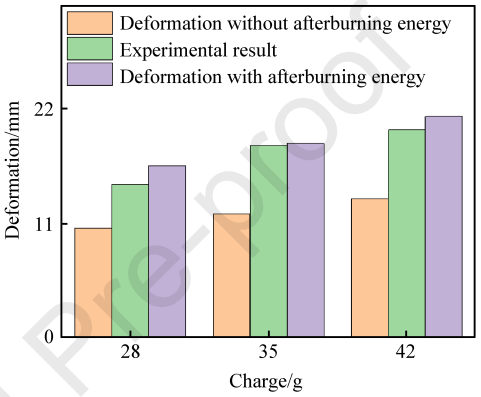

(d)

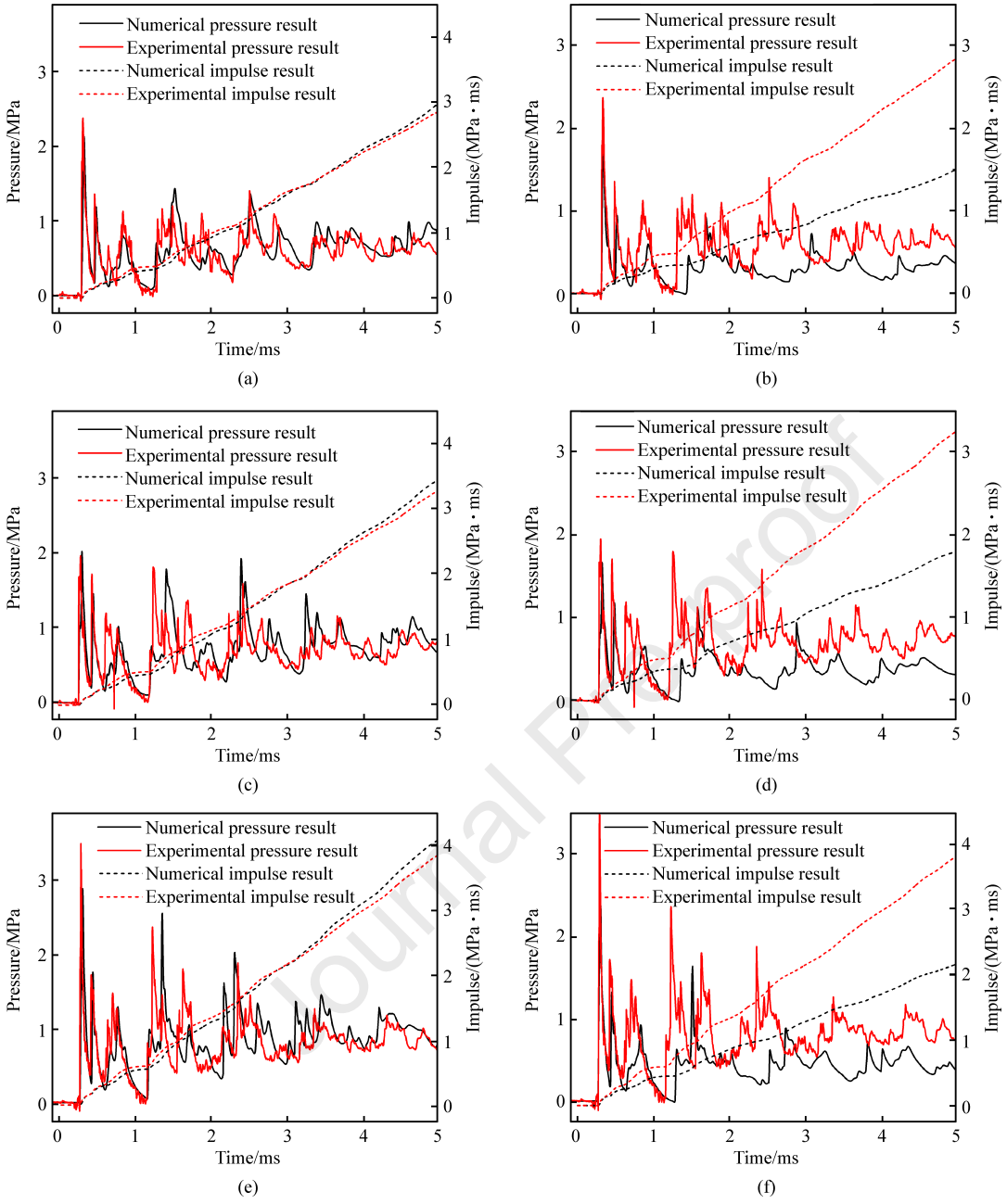

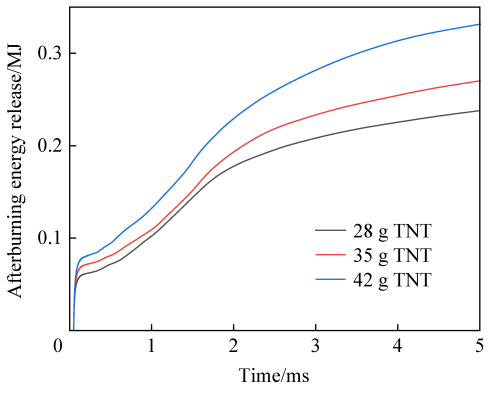

(a)

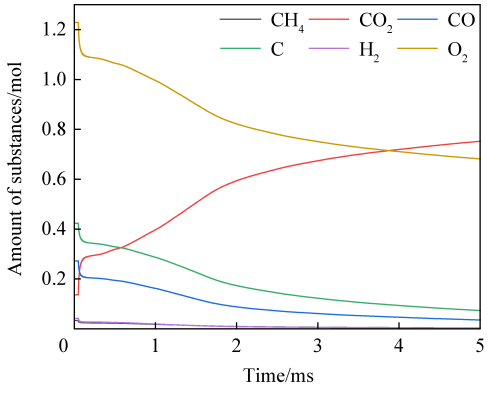

(b)

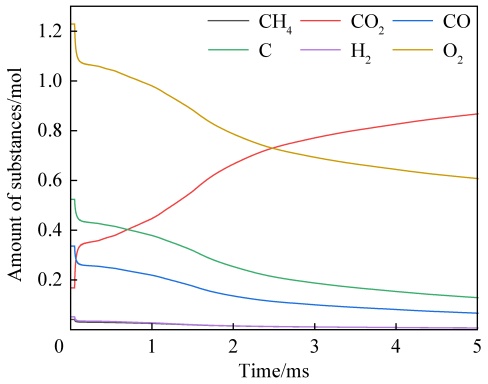

(c)

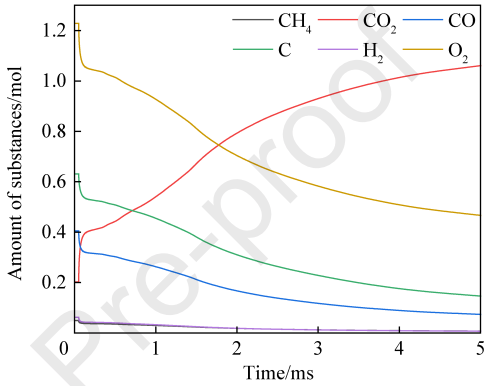

(d)

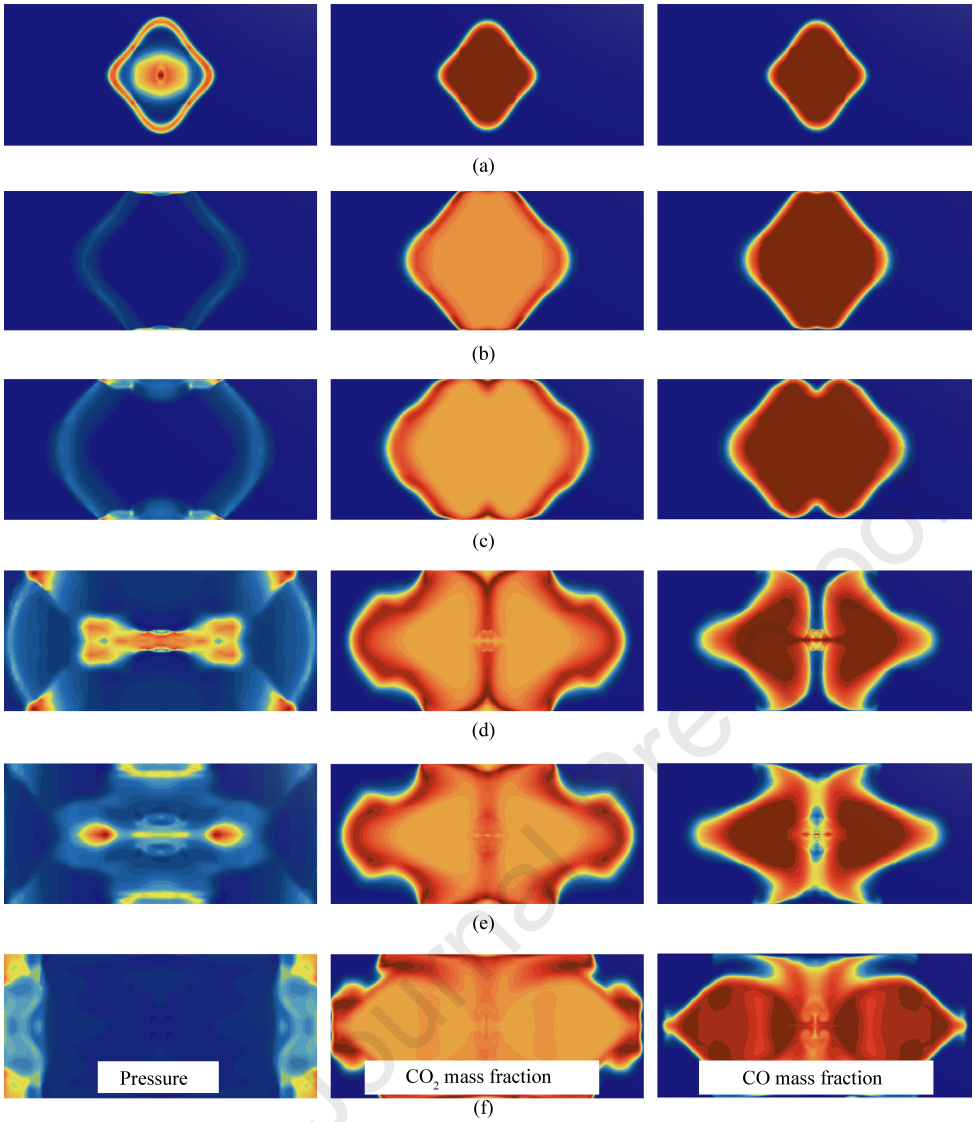

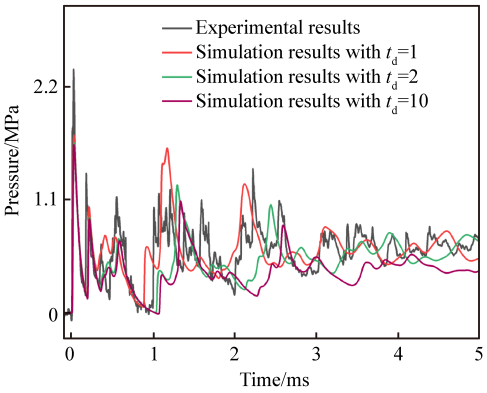

(a)

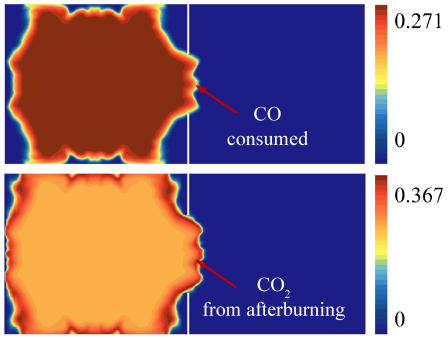

(b)

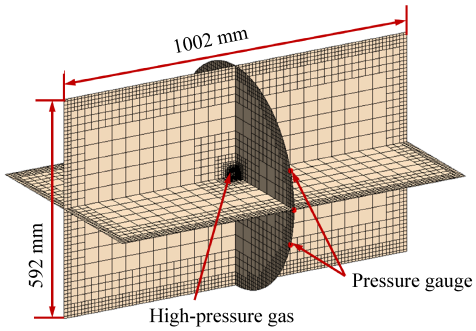

(c)

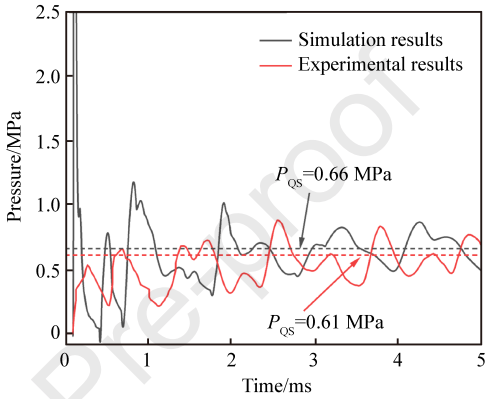

(d)

Conflict of Interest

The authors declare that they have no known competing financial interests or personal relationships that could have appeared to influence the work reported in this paper.